IEEE Access
Multidisciplinary | Rapid Review | Open Access Journal

SPECIAL SECTION ON ARTIFICIAL INTELLIGENCE FOR PHYSICAL-LAYER WIRELESS COMMUNICATIONS

Received March 21, 2019, accepted April 15, 2019, date of publication April 22, 2019, date of current version May 3, 2019.

Digital Object Identifier 10.1109/ACCESS.2019.2912321

A Novel MIMO Channel Model for Congested Communication Environments

DENGHONG TANG[1], XIAOLI XI[1], AND JIE ZHOU[2], (Senior Member, IEEE)
[1]Institute of Advanced Navigation and Electromagnetics, Xi'an University of Technology, Xi'an 710048, China
[2]Department of Communications, Nanjing University of Information Science and Technology, Nanjing 210044, China

Corresponding author: Xiaoli Xi (xixiaoli@xaut.edu.cn)

This work was supported by the National Natural Science Foundation of China under Grant 61771389 and Grant 61701398.

ABSTRACT This paper presents a novel multiple-input multiple-output (MIMO) channel model for congested curved-street vehicle-to-vehicle (V2V) non-line-of-sight communication environments, where the scatterers are located within narrow arcs along the curved street. The mobile transmitter and mobile receiver are equipped with massive MIMO antenna array; therefore, three-dimensional spherical antenna arrays are introduced in the model, rather than two-dimensional planar wavefront assumption used in traditional MIMO channel models. The closed expressions for the probability density functions of the azimuth angle of departure, the elevation angle of departure, the azimuth angle of arrival, and elevation angle of arrival are first deduced by analyzing the proposed V2V channel model. We then analyze the temporal and spatial cross-correlation functions corresponding to the single- and doublebounced scattering propagation paths. Comparisons with previously reported results are used to validate the applicability and feasibility of the proposed model.

INDEX TERMS MIMO channel model, V2V communications, AoD and AoA estimation, crosscorrelation function.

I. INTRODUCTION

A. MOTIVATION

Recently,vehicle-to-vehicle (V2V) communications have been suggested as a promising technology for the development of fifth generation (5G) wireless communication networks [1]. Moreover, the combination of multiple-input multiple-output (MIMO) technologies with V2V wireless communication systems have received considerable attention because low-elevation multiple antennas can be easily employed on vehicular surfaces [2]. In V2V scenarios, the mobile transmitter (MT) and mobile receiver (MR) are in relative motion, therefore, the exact knowledge of the characteristics of fading channels is critical to the development of more stable and efficient V2V communication systems. Channel modeling has been recognized as an effective method for reliably describing the channel characteristics [3], [4].

B. PRIOR WORK

In [5]–[10], many two dimensional (2D) geometry-based channel models were reported, such as circular models, elliptical models, and hollow-disk models. Subsequently, an angular spread of the incident signals in three dimensional (3D) space because of the interaction of the waves by vertically disposed objects was observed by researchers in [11]–[16]. The authors in [11]–[14] proposed a series of 3D geometry-based scattering channel models for micro-cell environments; however, they did not discuss the time-varying characteristics of the MIMO channels. A 3D geometric channel model was constructed in [15] and [16], based on the cross-polarization identification for narrow-band wireless models, without considering the time-varying channel characteristics. The studies in [17] showed that the above-mentioned models could not be used to accurately describe the urban street V2V scattering environments, because the scattering distributions of those models were generally distributed around the transmitters or receivers, which belonged to omnidirectional scattering scenarios. Avazov and Patzold [18] and Zhou *et al.* [19] proposed statistical channel models for V2V communication systems based on standard street scattering, where the scatterers were evenly distributed in the form of rectangular lattices. More specifically, for a congested curved street environment, it is unreasonable to assume that the scattering distributions are in the form of straight lines because of the great influence

The associate editor coordinating the review of this manuscript and approving it for publication was Guan Gui.

of scattering distribution and the spatial structure on the outdoor MIMO channels [20], [21].

Recently, Jiang *et al.* [22] presented a 3D semi-ellipsoid scattering channel model for urban street V2V communication environments, in which a MIMO antenna array model was adopted to analyze the temporal and frequency statistical characteristics for the propagation channels. In fact, Hong *et al.* [23] and Hong and Kim [24] have carried out the research on the collision warning system in a curved street vehicle communication environment. However, the antennas applied in the aforementioned models are all assumed to be planar. For future urban V2V mobile communication environments, the propagation links are more complicated due to the position and configuration changes of the large-scale antennas. Therefore, the discussion on propagation links connecting different transmitting and receiving antennas should be undertaken in detail.

The authors in [25]–[28] proposed series of MIMO planar antenna arrays, such as the uniform linear array (ULA), uniform circular array (UCA), uniform rectangular array (URA), and the L-shaped array configurations. In the 5G MIMO technology high-capacity evaluation, Zhou *et al.* [29] developed an electromagnetic vector sensor, and applied it to the deterministic covariance matrix of the MIMO uniform concentric circular array (UCCA), at the transmitter and receiver. Recently, with the support from the METIS project, an increasing number of researchers have been focusing on large-scale MIMO channel modeling. For instance, Wu *et al.* [30] researched the near-field effects and non-stationarity of the MIMO antenna arrays. However, they did not consider the impact of the spherical wavefront and the time-variant properties on the non-line-of-sight (NLOS) components. For MIMO communication systems, Wu *et al.* [31] presented a theoretical non-stationary wide-band twin-cluster time-variant and array-variant elliptical channel model. The temporal cross-correlation functions (CCFs) for every propagation component were analyzed; however, the angular spread of the incident signals in the elevation plane was not included in detail. Nevertheless, these mentioned arrays are limited to 2D analyse and may be not applicable to general MIMO systems for the low spatial utilization and concern about antenna blockage from outer antennas. For the 3D MIMO channel modeling, the dimension attributes of the antenna array are expected to have great impacts on the overall channel performance. The channel statistics corresponding to the geometric transmission path lengths in 3D space change constantly as the elevation and azimuth angles vary for different delays.

C. MAIN CONTRIBUTIONS

In this paper, we present a novel massive MIMO channel model for congested curved-street V2V mobile communication environments. The mobile transmitter (MT) and mobile receiver (MR) of the proposed MIMO channel model are assumed to be equipped with 3D low-elevation spherical antenna arrays instead of the 2D planar wavefront assumption used in the traditional MIMO channel models. To evaluate the performance of the proposed multiantenna system, the spatial and temporal CCFs corresponding to the single- and double-bounced scattering propagation paths are presented. Moreover, the proposed model can describe a variety of V2V scenarios such as picocell, micro, and macro scenarios by adjusting the channel parameters. The main contributions of this paper are summarized as follows:

(1) We propose a MIMO fading channel model which can be used to design and evaluate the performance of future V2V communication systems. The time-varying properties of the proposed channel with respect to the relative motion between the transmitter and receiver are studied, including the angle of departure (AoD) and angle of arrival (AoA) statistics, the spatial and temporal cross-correlations.

(2) In the proposed model, we introduce a spherical wavefront assumption to model the NLOS congested environments in curved streets, which would benefit the research on developing more stable and efficient V2V communication systems.

(3) A 3D antenna array model is utilized for the evaluation of the V2V communication MIMO systems. The impact of the antenna spacing on the spatial correlation between different antenna elements is analyzed in detail.

The remainder of this paper is organized as follows. In Section II, the proposed MIMO geometric V2V channel model is discussed. Analysis of space and time CCFs on both the single- and double-bounced components is provided in Section III. In Section IV, numerical results are given and discussed. Our conclusions are presented in Section V.

II. PROPOSED MIMO GEOMETRIC V2V CHANNEL MODEL

For a typical standard street transmission scenario, Avazov and Patzold [18] proposed a vehicle-to-vehicle (V2V) communication-system channel model, wherein the transmitter impinges on effective scatterers (representing buildings and trees) before reaching the receiver. The scatterers were idealized as rectangular dots parallel to each side of the street. The model analyzed Doppler parameters and the impacts of street scatterers on the V2V communication system performance. The research in [9]- [11] has confirmed that the characteristics of outdoor channel models are greatly affected by the distribution pattern of the scatterers and the spatial structure of the models under discussion. Hence, the previously established models are thus no longer applicable to congested curved streets in the V2V communication scenario shown in [18]- [20]. For the typical NLOS V2V propagation scenario illustrated in Fig. 1, we present a novel 3D MIMO scattering model. Note that the occlusions are situated at the inner sides of the C-junctions, and the trees and buildings on the edge of the street are considered as scatterers. The MT is responsible for the transmitted signal and the MR is responsible for the received signal.

Moreover, several basic assumptions as given in [12] and [18]–[20], are utilized to make the MIMO channel model more systematic and matched with the congested curved-street V2V communication environments. (1) The

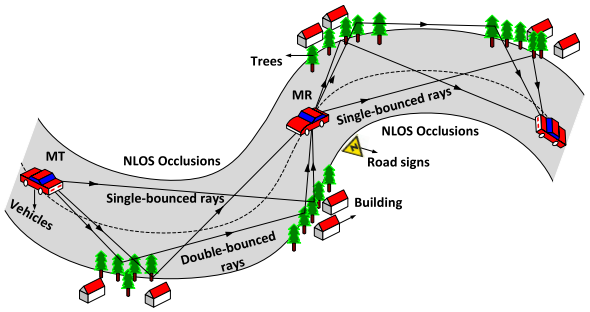

FIGURE 1. Typical NLOS V2V mobile communication environment and its scattering channel model.

scattering region is limited within the arc of the street edge, and the influence of rough street surface is not considered. (2) The same scattering coefficient and uniform stochastic phases are attached to all scatterers which are independent of each other. (3) The data have shown that single-bounced and double-bounced rays have been detected for the city V2V channels [20]; therefore, the effects of the above two scattering mechanisms are studied without considering other scattering mechanisms.

Fig. 2 illustrates the geometric properties and movement statistics of the single-bounced mechanism in the azimuth plane for the C-junction scattering model. The complex 3D figures corresponding to the MIMO antennas are omitted for brevity. Note that the entire NLOS V2V mobile scenarios can be approximately visualized as a standard geometric semicircle structure. Herein, the definition of fundamental parameters is given in Tab.1. For V2V scenarios, MT and MR are both moving, therefore, the scenario can be considered equivalent to a static MT and a relatively moving MR in an arbitrary direction ϕ_R with a speed v_R for simplicity, as shown in Fig. 3. To analyze the proposed C-junction scattering model, we describe a 3D MIMO antenna array model, as illustrated in Fig. 4. We first discuss the general space auto-correlation function (ACF) of the proposed large-scale antennas, the time-varying geometric path lengths, as well as the spatial characteristics of the proposed non-stationary radio channels are then performed.

A. PROPOSED 3D MASSIVE MIMO ANTENNA ARRAY

Herein, we propose a spherical vehicular MIMO antenna array model, as shown in Fig. 4. In this case, the signal spherical wavefront assumption is proposed, moreover, the channel impulse response of MIMO antenna arrays can be separated into steering-vector-dependent components and time-dependent [6], which can be expressed as

$$\mathbf{h}(t) = \sum_{p=1}^{P} a_p(t)\Psi\left(\Theta_p, \mathbf{g}_p\right) \tag{1}$$

where P denotes the number of large-scale antennas and $p = 1, 2, 3, \ldots, P$, $\Psi(\Theta_p, \mathbf{g}_p)$ denotes the steering vector of the compact antenna array, in which the spatial vector parameters are given as $\Theta = [\theta, \varphi]^T$ and $\mathbf{g} = [\gamma, \eta]^T$. The azimuth and elevation angles with respect to the x- and z-axes are denoted by scalars $0 \le \varphi \le 2\pi$ and $-\pi/2 \le \theta \le \pi/2$, respectively. Moreover, the polarization phase difference and the auxiliary polarization angle are respectively denoted by the scalars $-\pi \le \eta \le \pi$ and $0 \le \gamma \le 2\pi$. $a_p(t)$ represents a set of zero-mean complex random variables which are independent identically distributed. Then under the assumption that the antenna elements are vertically polarized, we can express the steering vector for the proposed array model can be expressed as

$$\begin{aligned}\mathbf{a}(\theta, \varphi) = \Big[& e^{j\zeta \cos(\varphi-\varphi_1)\sin(\theta-\theta_1)}, e^{j\zeta \cos(\varphi-\varphi_2)\sin(\theta-\theta_2)}, \\ & \ldots, e^{j\zeta \cos(\varphi-\varphi_p)\sin(\theta-\theta_p)}, \\ & \ldots, e^{j\zeta \cos(\varphi-\varphi_P)\sin(\theta-\theta_P)}\Big]\end{aligned} \tag{2}$$

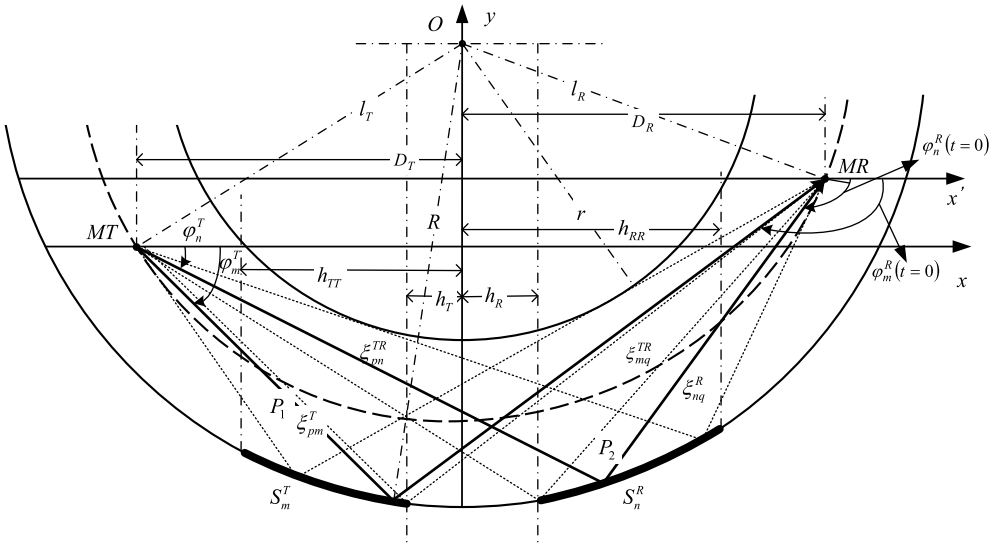

FIGURE 2. Geometric angles and transmission path lengths of the V2V channel model illustrating the single-bounced scattering mechanism.

TABLE 1. Definition of parameters.

Parameter	Definition
O	The center of the semicircular model
r,R	The inner and outer radii, respectively
$l_T(l_R)$	The distance from MT (MR) to the center O
$D_T(D_R)$	The initial distance from MT (MR) to the y-axis
h_T,h_{TT},h_R,h_{RR}	The distances from both sides of the scattering area edge to the y-axis
M, N	The number of scatterers
$S_m^T\ (m=1,2,...,M)$,$S_n^R\ (n=1,2,...,N)$	Arc-distributed scatterers close to MT and MR, respectively
$\varphi_m^T(\varphi_n^T)$, $\theta_m^T(\theta_n^T)$	Azimuth and elevation angles propagated via the scatterer S_m^T (S_n^R) at MT
$\varphi_m^R(\varphi_n^R)$, $\theta_m^R(\theta_n^R)$	Azimuth and elevation angles propagated via the scatterer S_m^T (S_n^R) at MR

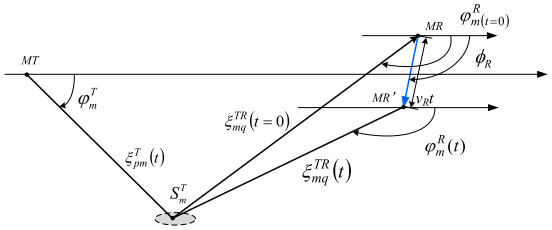

FIGURE 3. Time-varying parameters in the V2V channel model.

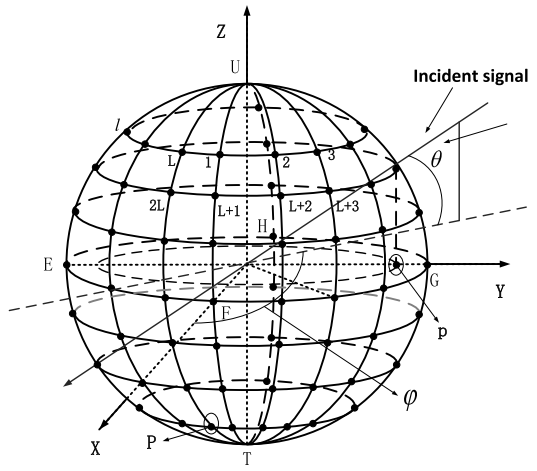

FIGURE 4. Proposed 3D vehicular MIMO antenna array.

where the superscript $[\cdot]^T$ stands for the transpose and the phase steering for the p-th element is denoted by $a_p(\theta,\varphi) = e^{j\zeta\cos(\varphi-\varphi_p)\sin(\theta-\theta_p)}$, $\zeta = 2\pi\frac{R_S}{\lambda}$, where R_S represents the radius of the spherical array and λ represents the signal wavelength.

In the proposed model, the omnidirectional spherical antennas receive signal wavefront emitted from the 3D clusters. We therefore present the entire vehicular antenna system as a 3D space spherical box with orderly arranged antenna array elements. Furthermore, in order to realize the proposed 3D MIMO system, we number each antenna element according to the positions of each antenna element on the faces of the hemispheres, as shown in Fig. 5.

Let us define $V = 2L$ as the number of meridional rings and W as the number of zonal rings of the proposed vehicular antenna array model. Hence, the number of the MIMO antenna elements is $P = 2\times V\times M$. Further, we set the number to $P = Q = 208$ (i.e., $V = 8$, $W = 13$). According to the upper and lower hemispherical array structures, the initial phase of the p-th element can be expressed as

$$\varphi_p = 2\pi\frac{l-1}{L},\quad l = 1,2,\ldots,\ p-\left\lfloor\frac{p}{L}\right\rfloor\times L,\ldots,L \tag{3}$$

$$\theta_p = \frac{\pi}{W+1}\left(\frac{W+1}{2}-w\right),\quad w = 1,2,\ldots\left\lceil\frac{p}{L}\right\rceil,\ldots,W \tag{4}$$

Please note that the expression in (2) assumes that the MR antennas are in the near field of the MT antennas. Thus, the general space auto-correlation function with respect to the p-th and q-th elements can be defined as

$$\begin{aligned}\rho(p,q) &= \frac{E\left\{\left(h_p-\widetilde{h}_p\right)\left(h_q-\widetilde{h}_q\right)\right\}}{\sqrt{E\left\{\left(h_p-\widetilde{h}_p\right)^2\right\}E\left\{\left(h_q-\widetilde{h}_q\right)^2\right\}}}\\ &= \frac{\int_\varphi\int_\theta \mathbf{a}_p(\theta,\varphi)\,\mathbf{a}_q^*(\theta,\varphi)\sin(\theta)f(\theta,\varphi)\,d\theta d\varphi}{\sqrt{\int_\varphi\int_\theta\left|\mathbf{a}_p(\theta,\varphi)\right|^2\sin(\theta)f(\theta,\varphi)\,d\theta d\varphi}}\\ &\quad\times\frac{1}{\sqrt{\int_\varphi\int_\theta\left|\mathbf{a}_q(\theta,\varphi)\right|^2\sin(\theta)f(\theta,\varphi)\,d\theta d\varphi}}\end{aligned} \tag{5}$$

where $E[\cdot]$ denotes the expectation, the superscript $(\cdot)^*$ is the complex conjugate, the scalar $\widetilde{h}_p$ is the mean value of the channel impulse response at antenna p, and the scalar $f(\theta,\varphi)$ is the joint probability density function (PDF) of the AoD of the multipath signal in 3D space [22]. For the proposed 3D large-scale arrays, we assume the incident signals are uniformly distributed in the elevation and azimuth planes, then (5) can be rewritten as:

$$\begin{aligned}\rho(p,q) = \frac{1}{\pi}\int_0^{2\pi}\int_0^{\pi/2} & e^{j2\pi\frac{R_S}{\lambda}\cos(\varphi-\varphi_p)\sin(\theta-\theta_p)}\\ &\times e^{j2\pi\frac{R_S}{\lambda}\cos(\varphi-\varphi_q)\sin(\theta-\theta_q)}\sin\theta\,d\theta\,d\varphi\end{aligned} \tag{6}$$

B. GEOMETRIC PROPERTIES OF THE V2V COMMUNICATION ENVIRONMENTS

Here in our proposed V2V MIMO scattering model, the moving MT and MR are both equipped with the spherical antenna

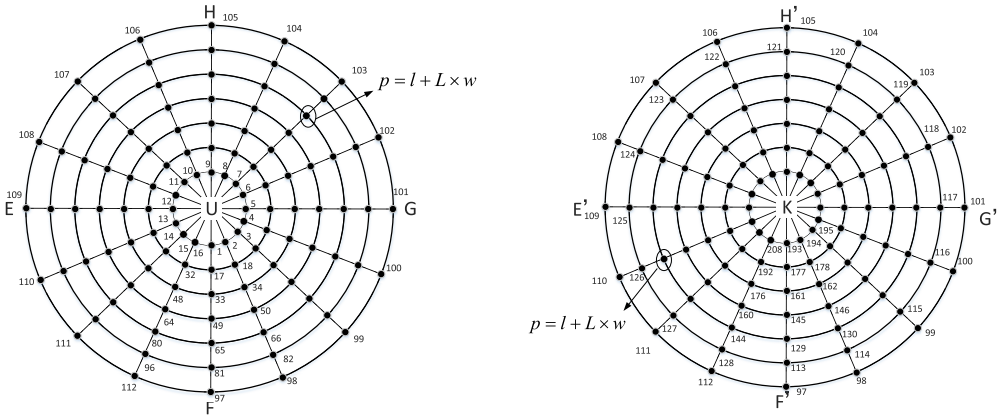

FIGURE 5. Layout of the proposed MIMO antenna elements: (a) upper hemisphere U-EFGH; (b) lower hemisphere EFGH-T.

arrays; the numbers of antenna elements are P and Q and the spherical radii are r_T and r_R, respectively. Thus, we can describe the proposed non-stationary V2V channels with the time-variant path length functions [32], specially, when the variable $t = 0$, the proposed model has wide-sense stationary channels [6], [7]. For the single-bounced path P_1 at time t, $\xi_{pmq}(t)$ represents the distance from transmit antenna element $A_p^T (p = 1, 2, \ldots, P)$ to receiving antenna element A_q^R $(q = 1, 2, \ldots, Q)$ via scatterer S_m^T, which can be expressed as $\xi_{pmq}(t) = \xi_{pm}^T(t) + \xi_{mq}^{TR}(t)$. $\xi_{pm}^T(t)$ is the distance between the transmit antenna element A_p^T and the scatterer which can be derived as a function of the angles φ_m^T and θ_m^T based on Fig. 6.

$$\xi_{pm}^T(t) = \sqrt{r_T^2 \sin^2\theta_p + k_1^2 + k_2^2 - 2k_1k_2\cos(\varphi_m^T - \varphi_p)} \quad (7)$$

where k_1 equals to the distance from the MT antenna center to the scatterer and can be derived based on Fig. 2

$$k_1 = \cos\left(\varphi_m^T - \varphi_p + \arccos\frac{r_T}{D_T}\right) + \sqrt{\left[\cos^2\left(\varphi_m^T - \varphi_p + \arccos\frac{r_T}{D_T}\right) + 1\right]l_T^2 - R^2} \quad (8)$$

$$k_2 = r_T \sin\theta_p / \tan\theta_m^T \quad (9)$$

Moreover, $\xi_{mq}^{TR}(t)$ represents the distance between the scatterer to the receiving antenna element A_q^R and can be derived as

$$\xi_{mq}^{TR}(t) = \sqrt{r_R^2 \sin^2\theta_q + k_1^3 + k_2^4 - 2k_3k_4\cos(\varphi_m^R - \varphi_q)} \quad (10)$$

where

$$k_3 = r_R \sin\theta_q / \tan\theta_m^R \quad (11)$$

$$k_4 = \sqrt{(D_T + D_R - \xi_{pm}^T(t)\cos\varphi_m^T - v_R t\cos\varphi_R)^2 + k_5^2} \quad (12)$$

$$k_5 = \xi_{pm}^T(t)\sin\varphi_m^T + \sqrt{l_T^2 - D_T^2} - \sqrt{l_R^2 - D_R^2} \quad (13)$$

It is true that, for the single-bounced path P_2, $\xi_{pnq}(t) = \xi_{pn}^{TR}(t) + \xi_{nq}^R(t)$ can express the distance from the transmit antenna element A_p^T to the receiving antenna element A_q^R via the scatterer S_n^T at time t, and

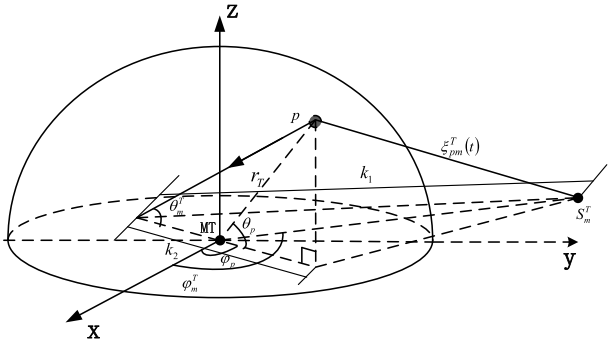

FIGURE 6. Geometric angles and path lengths based on the proposed 3D antenna receiver.

$$\xi_{pn}^{TR}(t) = \sqrt{r_T^2 \sin^2\theta_p + k_6^2 + k_7^2 - 2k_6k_7\cos(\varphi_n^T - \varphi_p)} \quad (14)$$

$$\xi_{nq}^R(t) = \sqrt{r_R^2 \sin^2\theta_q + k_8^2 + k_9^2 - 2k_8k_9\cos(\varphi_n^R - \varphi_q)} \quad (15)$$

where

$$k_6 = \cos\left(\varphi_n^R - \varphi_p + \arccos\frac{r_T}{D_T}\right) + \sqrt{\left[\cos^2\left(\varphi_n^R - \varphi_p + \arccos\frac{r_T}{D_T}\right) + 1\right]l_T^2 - R^2} \quad (16)$$

$$k_7 = r_T \sin\theta_p / \tan\theta_n^T \quad (17)$$

$$k_8 = r_R \sin\theta_q / \tan\theta_n^R \quad (18)$$

$$k_9 = \sqrt{(D_T + D_R - \xi_{pn}^{TR}(t)\cos\varphi_n^T - v_R t\cos\varphi_R)^2 + k_{10}^2} \quad (19)$$

$$k_{10} = \xi_{pn}^{TR}(t)\sin\varphi_n^T + \sqrt{l_T^2 - D_T^2} - \sqrt{l_R^2 - D_R^2} \quad (20)$$

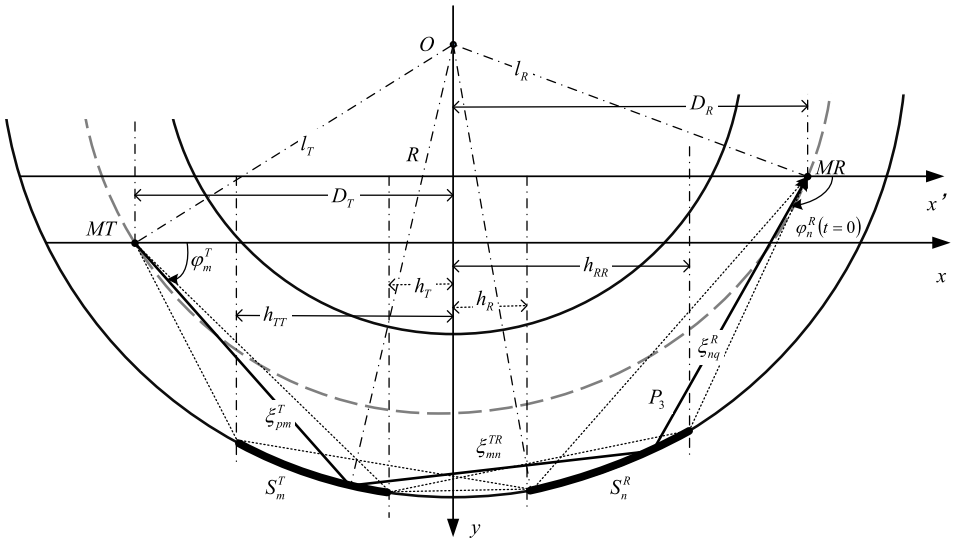

FIGURE 7. Geometric angles and path lengths based on the proposed 3D antenna receiver.

Similarly, Fig. 7 illustrates the geometric properties and moving statistics for the double-bounced mechanism in the azimuth plane for the proposed MIMO V2V scattering model. The signals transmits trough two times of scattering via S_m^T and S_n^R to the receiver. Thus, for the double-bounced path P_3 at time t, the distance between transmitting antenna element A_p^T and receiving antenna element A_q^R via the scatterers S_m^T and S_n^R at time t can be expressed as $\xi_{pmnq}(t) = \xi_{pm}^T(t) + \xi_{mn}^{TR}(t) + \xi_{nq}^R(t)$, where $\xi_{pm}^T(t)$ and are given by (7) and (15), respectively, and

$$\xi_{mn}^{TR}(t) = 2R\sin\left\{\frac{1}{2}\times\left[\arcsin\frac{r_T}{D_T}+\arcsin\frac{r_R}{D_R} - \arcsin\frac{k_1\sin(\arccos\frac{D_T}{l_T}+\varphi_m^T)}{R} - \arcsin\frac{k_9\sin(\varphi_n^R-\arccos\frac{D_R}{l_R})}{R}\right]\right\} \tag{21}$$

III. CHANNEL CHARACTERISTICS OF THE PROPOSED MODEL

A. SPATIAL CHARACTERISTICS OF THE RADIO CHANNEL

Based on the single- and double-bounced scattering mechanisms for the proposed V2V channels, the AoD and AoA PDFs measured in the azimuth and elevation planes can be derived. The Gaussian, Laplacian, and von Mises distributions have been reported in [7] to be used to characterize the geometry-based MIMO channel models. When the number of scatterers $M, N \to \infty$, the discrete random angle variables φ_m^T, θ_m^T, φ_m^R, and θ_m^R are replaced by the continuous random variables φ_T,θ_T, φ_R, and θ_R [9]. Considering the peculiarity of the urban congested curved-street environment, most of the scatterers in the model are distributed along the arc area, and the density of the scattering gradually decreases as the distance between the transmitter and receiver increases. Hence, we adopt the Gaussian distribution in the modeling of scatterers for our proposed model, because it is used in many typical channels for the evaluation of spatial characteristics. The spatial Gaussian distribution density function is expressed as

$$f(\xi,\sigma) = \frac{1}{2\pi\sigma^2}\times\exp\left(-\xi^2/2\sigma^2\right) \tag{22}$$

where σ is the standard deviation. Then, by transforming the Cartesian coordinate (x, y, z) to the polar coordinate (ξ, φ, θ), the joint PDF of the AoD for the single-bounced mechanism P_1 can be written as

$$\begin{aligned} f\left(\xi_{pm}^T(t),\varphi_T,\theta_T\right) &= \frac{f(x,y,z)}{|J(x,y,z)|}\left|\begin{cases} x=\xi_{pm}^T(t)\ \cos\theta_T\sin\varphi_T - D_T \\ y=\xi_{pm}^T(t)\ \cos\theta_T\sin\varphi_T - D_T \\ z=\xi_{pm}^T(t)\ \sin\theta_T \end{cases}\right. \\ &= \frac{\left(\xi_{pm}^T(t)\right)^2\cos\theta_T}{2\pi\sigma^2} \times\exp\left\{-\frac{1}{2\sigma^2}\left[\left(\xi_{pm}^T(t)\ \cos\theta_T\sin\varphi_T - D_T\right)^2 + \left(\xi_{pm}^T(t)\ \cos\theta_T\cos\varphi_T\right)^2 + \left(\xi_{pm}^T(t)\ \sin\theta_T\right)^2\right]\right\} \end{aligned} \tag{23}$$

where $J(x, y, z)$ is the Jacobian of the inverse transformation. As mentioned in [11], in the MIMO channel model, the AoA is often associated with the corresponding emission angle AoD. Thus, the joint PDF of the AoA for the single-bounced mechanism P_1 can be derived as

$$\begin{aligned} f\left(\xi_{mq}^{TR}(t),\varphi_R,\theta_R\right) &= \frac{\left(\xi_{mq}^{TR}(t)\right)^2\cos\theta_R}{2\pi\sigma^2} \times\exp\left\{-\frac{1}{2\sigma^2}\left[\left(\xi_{mq}^{TR}(t)\ \cos\theta_R\sin\varphi_R - D_R\right)^2 + \left(\xi_{mq}^{TR}(t)\ \cos\theta_R\cos\varphi_R\right)^2 + \left(\xi_{mq}^{TR}(t)\ \sin\theta_R\right)^2\right]\right\} \end{aligned} \tag{24}$$

Herein, by integrating the joint PDFs in (23) and (24) over the entire angle path length, the marginal AoD and AoA PDFs are given by

$$f(\varphi_T, \theta_T) = \int_{\xi^T_{\min}}^{\xi^T_{\max}} f\left(\xi^T_{pm}(t), \varphi_T, \theta_T\right) d\xi \tag{25}$$

and

$$f(\varphi_R, \theta_R) = \int_{\xi^R_{\min}}^{\xi^R_{\max}} f\left(\xi^{TR}_{mq}(t), \varphi_R, \theta_R\right) d\xi \tag{26}$$

respectively.

Based on the model in Fig. 1, and considering the actual position of the MR, the boundary distances of the propagation path, $\xi^T_{pm}(t)$ and $\xi^{TR}_{mq}(t)$, are completely determined by the size of the scattering arc region. That is, the maximum and minimum values of the propagation path, $\xi^T_{\max}$, $\xi^T_{\min}$ and $\xi^R_{\max}$, $\xi^R_{\min}$, can be obtained from the boundary angles determined by the scattering areas h_T and h_R, and h_{TT} and h_{RR}, respectively. The same method can be used to derive the expressions of the marginal AoD and AoA PDFs for the single-bounced mechanism P_2 and double-bounced mechanism P_3 components.

B. TEMPORAL AND SPATIAL CROSS-CORRELATION FUNCTION

The study on the temporal and spatial characteristics is necessary for accommodating MIMO systems with the orthogonal frequency division multiplexing technology. The MT and MR of our model are both equipped with a large-scale version of the proposed vehicular MIMO antenna with P and Q omnidirectional elements, respectively. Therefore, unlike the traditional MIMO channel models, the time-varying propagation link p-q connecting element A^T_p and element A^R_q for our proposed model is assumed as spherical. In this case, the temporal and spatial CCFs could be completely determined by the $P \times Q$ channel matrix $\mathbf{H}(t, \tau) = [h_{pq}(t, \tau)]_{P\times Q}$, where the multipath channel impulse response containing the single-bounced component SBM and SBN, and the double-bounced component DB can be expressed as

$$h_{pq}(t) = h^{SBM}_{pq}(t) + h^{SBN}_{pq}(t) + h^{DB}_{pq}(t) \tag{27}$$

where

$$h^{SBM}_{pq}(t) = \lim_{M\to\infty} \sqrt{\frac{\eta_{SBN}}{M}} \sum_{m=1}^{M} g_m \times e^{j\left[-\frac{2\pi\xi_{pmq}(t)}{\lambda} + \varpi_m + (\omega^T_m + \omega^R_m)t\right]} \tag{28}$$

$$h^{SBN}_{pq}(t) = \lim_{N\to\infty} \sqrt{\frac{\eta_{SBN}}{N}} \sum_{n=1}^{N} g_{mn} \times e^{j\left[-\frac{2\pi\xi_{pmnq}(t)}{\lambda} + \varpi_{mn} + (\omega^T_m + \omega^R_n)t\right]} \tag{29}$$

$$h^{DB}_{pq}(t) = \lim_{M,N\to\infty} \sqrt{\frac{\eta_{DB}}{MN}} \sum_{m=1}^{M}\sum_{n=1}^{N} g_n \times e^{j\left[-\frac{2\pi\xi_{pnq}(t)}{\lambda} + \varpi_n + (\omega^T_n + \omega^R_n)t\right]} \tag{30}$$

In the equations above, $\omega^T_m = 2\pi f^T_{\max}\cos\varphi^T_m\cos\theta^T_m$, $\omega^T_n = 2\pi f^T_{\max}\cos\varphi^T_n\cos\theta^T_n$, $\omega^R_m = 2\pi f^R_{\max}\cos(\phi_R - \varphi^R_m)\cos\theta^R_m$, and $\omega^R_n = 2\pi f^R_{\max}\cos(\phi_R - \varphi^R_n)\cos\theta^R_n$. The symbols $f^T_{\max}$ and $f^R_{\max}$ denote the maximum Doppler frequencies for the MT and MR, respectively. The parameters η_{SBM}, η_{SBN}, and η_{DB} define the mean powers for each component, which satisfy the normalization condition. Moreover, g_m, g_n, and g_{mn} represent the amplitudes of the signals after scattering. ϖ_m, ϖ_n, and ϖ_{mn} are independent and identically Gaussian distributed random variables over $[0, 2\pi]$.

Herein, the multipath channel impulse response for the propagation link $p' - q'$ connecting element $A^T_{p'}$ and element $A^R_{q'}$ is defined as $h_{p'q'}(t)$, then, the normalized temporal CCF between link $p - q$ and link $p' - q'$ at different time instants t is defined as

$$\begin{aligned} R_{pq,p'q'}(t,\tau) &= E\left[\frac{h_{pq}(t)\, h^*_{p'q'}(t-\tau)}{|h_{pq}(t)|\,|h^*_{p'q'}(t-\tau)|}\right] \\ &= \eta_{SBM}\lim_{M\to\infty}\frac{1}{M}\sum_{m=1}^{M}\Big(E[g^2_m] \\ &\quad\times e^{j(\omega^T_m+\omega^R_m)\tau - \frac{j2\pi\left[\xi_{pmq}(t)-\xi_{p'mq'}(t)\right]}{\lambda}}\Big) \\ &\quad+\eta_{SBN}\lim_{N\to\infty}\frac{1}{N}\sum_{n=1}^{N}\Big(E[g^2_n] \\ &\quad\times e^{j(\omega^T_n+\omega^R_n)\tau - \frac{j\,2\pi\left[\xi_{pnq}(t)-\xi_{p'nq'}(t)\right]}{\lambda}}\Big) \\ &\quad+\eta_{DB}\lim_{M,N\to\infty}\frac{1}{MN}\sum_{m=1}^{M}\sum_{n=1}^{N}\Big(E[g^2_{mn}] \\ &\quad\times e^{j(\omega^T_m+\omega^R_n)\tau - \frac{j2\pi\left[\xi_{pmnq}(t)-\xi_{p'mnq'}(t)\right]}{\lambda}}\Big) \end{aligned} \tag{31}$$

where $*$ represents the complex conjugate. τ denotes the propagation delay of any one multipath signal in 3D space, specially, the longest and shortest propagation delays are respectively defined as $\tau_{\max}$ and $\tau_{\min}$, i.e., $\tau_{\max} = \xi_{\max}/c_0$ and $\tau_{\min} = \xi_{\min}/c_0$, where c_0 denotes the propagation speed of signals, as shown in [11].

For a further analysis of the performance of the MIMO V2V channels, we use the same method as in [9] and [20]. For the single-bounced component P_1, the infinitesimal power related to the differential of the 3D angles $d\varphi_R$ and is proportional to $f(\varphi_R, \theta_R)d\varphi_R d\theta_R$. In the limit $M, N \to \infty$, this contribution must be equal to $E[g^2_m]/M$, i.e., $E\left[g_m{}^2\right]/M = f(\varphi_R, \theta_R)\, d\varphi_R d\theta_R$, Similarly, for the single-bounced component P_2, $E\left[g_n{}^2\right]/N = f(\phi_{R2}, \theta_{R2})\, d\varphi_{R2} d_{R2}$, where $f(\varphi_{R2}, \theta_{R2})$ denotes the AoA PDFs observed at the MR, and for the double-bounced component P_3, $E\left[g_{mn}{}^2\right]/MN = f(\varphi_T, \theta_T) f(\varphi_{R2}, \theta_{R2})\, d\varphi_{R2} d_{R2} d\varphi_T d\theta_T$. Therefore, the temporal CCF can be rewritten as follows:

$$\begin{aligned} &R_{pq,p'q'}(t,\tau) \\ &= \eta_{SBM}\int_{-\pi/2}^{\pi/2}\int_{0}^{2\pi} e^{-\frac{j2\pi\left[\xi_{pmq}(t)\ -\xi_{p'mq'}(t)\right]}{\lambda}} \end{aligned}$$

$$\times e^{j(\omega_m^T+\omega_m^R)\tau} \times f(\varphi_R,\theta_R)d\varphi_R d\theta_R$$
$$+\eta_{SBN}\int_{-\pi/2}^{\pi/2}\int_0^{2\pi} e^{-\frac{j\,2\pi\left[\xi_{pnq}(t)\ -\xi_{p'nq'}(t)\right]}{\lambda}}$$
$$\times e^{j(\omega_n^T+\omega_n^R)\tau} \times f(\varphi_{R2},\theta_{R2})d\varphi_{R2}d\theta_{R2}$$
$$+\eta_{DB}\int_{-\pi/2}^{\pi/2}\int_0^{2\pi}\int_{-\pi/2}^{\pi/2}\int_0^{2\pi}$$
$$\times\ e^{j(\omega_m^T+\omega_n^R)\tau-\frac{j2\pi\left[\xi_{pmnq}(t)\ -\xi_{p'mnq'}(t)\right]}{\lambda}}$$
$$\times f(\varphi_T,\theta_T)f(\varphi_{R2},\theta_{R2})d\varphi_{R2}d_{R2}d\varphi_T d\theta_T \qquad (32)$$

Obviously, not only the geometric path lengths but also the moving properties will influence the temporal cross-correlation of the MIMO channels. Furthermore, the spatial CCF can be obtained from (32) by setting $t, \tau = 0$, as follows:

$$R_{pq,p'q'}(r_T, r_R)$$
$$= \eta_{SBM}\int_{-\pi/2}^{\pi/2}\int_0^{2\pi} e^{-\frac{j2\pi\left[\xi_{pmq}(t)-\xi_{p'mq'}(t)\right]}{\lambda}}$$
$$\times f(\varphi_R,\theta_R)d\varphi_R d\theta_R$$
$$+\eta_{SBN}\int_{-\pi/2}^{\pi/2}\int_0^{2\pi} e^{-\frac{j\,2\pi\left[\xi_{pnq}(t)\ -\xi_{p'nq'}(t)\right]}{\lambda}}$$
$$\times f(\varphi_{R2},\theta_{R2})d\varphi_{R2}d\theta_{R2}$$
$$+\eta_{DB}\int_{-\pi/2}^{\pi/2}\int_0^{2\pi}\int_{-\pi/2}^{\pi/2}\int_0^{2\pi} e^{-\frac{j2\pi\left[\xi_{pmnq}(t)\ -\xi_{p'mnq'}(t)\right]}{\lambda}}$$
$$\times f(\varphi_T,\theta_T)f(\varphi_{R2},\theta_{R2})d\varphi_{R2}d_{R2}d\varphi_T d\theta_T \qquad (33)$$

IV. NUMERICAL RESULTS AND DISCUSSION

In this section, we present analyses of the main theoretical results and their comparisons with some conventional models and measurements found in the literature (namely, [7], [19], [21], [29], and [33]) to further verify the reliability of the proposed MIMO V2V channel model. Moreover, in the simulation, the parameters are set as: $l_T = l_R = 40$ m, and $r = 30$ m, $R = 50$ m, $\eta_{SBM} = \eta_{SBN} = \eta_{DB} = 1/3$.

A. SPACE AUTO-CORRELATION PERFORMANCE

Fig. 8 presents the numerical SACFs with respect to the variation antenna elements for the proposed 3D MIMO antenna arrays. Note that with an increase in the antenna spacing R_S/λ, the SACFs decrease rapidly and eventually reach a relatively stable saturation value, which confirms the results in [29]. Moreover, for the areas of the upper and lower hemispheres seen in Fig. 5, as the receiving element changes from 2 to 200, the spatial fading correlations tend to decrease because of the continuously changing relative position between the two elements. From the simulation results, we can deduce that the proposed 3D MIMO antenna array model can effectively reduce the spatial fading correlations of the compact antenna systems, which can be further applied to modeling future V2V communications.

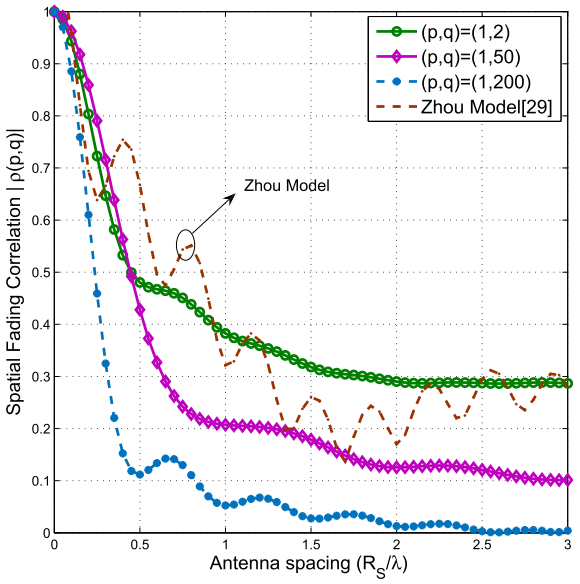

FIGURE 8. Spatial fading correlations concerning the variations in antenna elements.

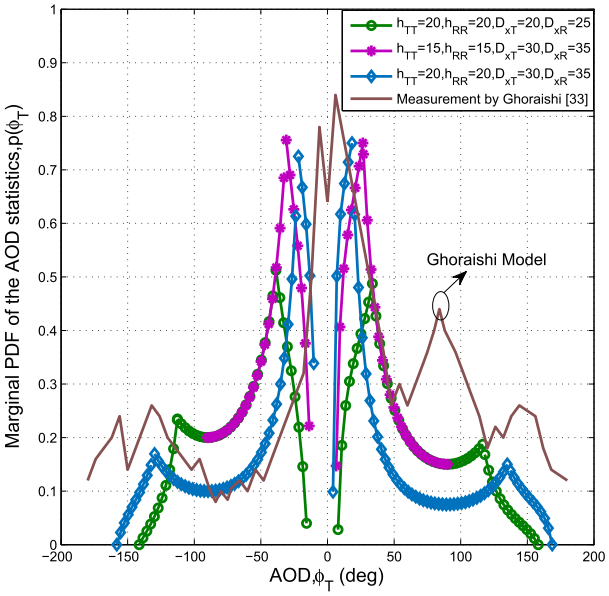

FIGURE 9. PDFs of the AoD statistics in the azimuth plane when $h_T = h_R = 5$ m.

B. AOD AND AOA STATISTICS ANALYSIS

In the simulation of angles φ_T and φ_R, we consider both the forward and the reverse link, which are respectively represented by the positive and negative semi-axis azimuth angles in Figs. 9 and 10. The MT is responsible for the transmitted signal in the forward link and the MR is responsible for the transmitted signal in the reverse link [19]. The PDFs of the AoD in regard to the initial distances D_T and D_R and the scattering areas h_{TT} and h_{RR} in the azimuth plane are presented in Fig. 9. It can be seen from the figure that, when $|\varphi_T|$ increases, the AoD probability density distribution first

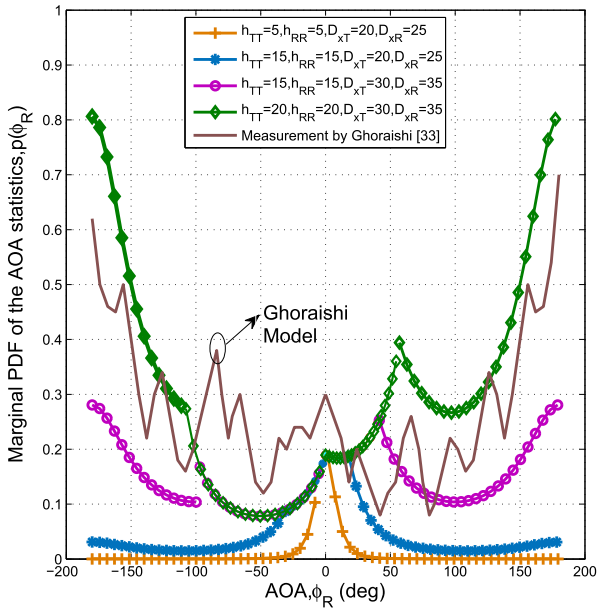

FIGURE 10. PDFs of the AoA statistics in the azimuth plane when $h_T = h_R = 5$ m.

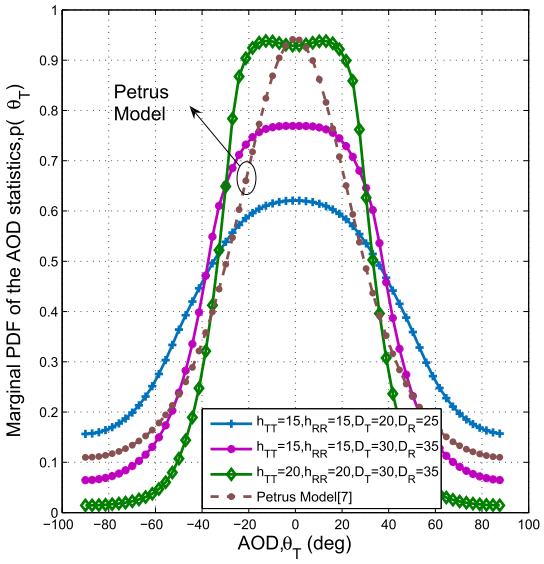

FIGURE 11. PDFs of the AoD statistics in the elevation plane when $h_T = h_R = 5$ m.

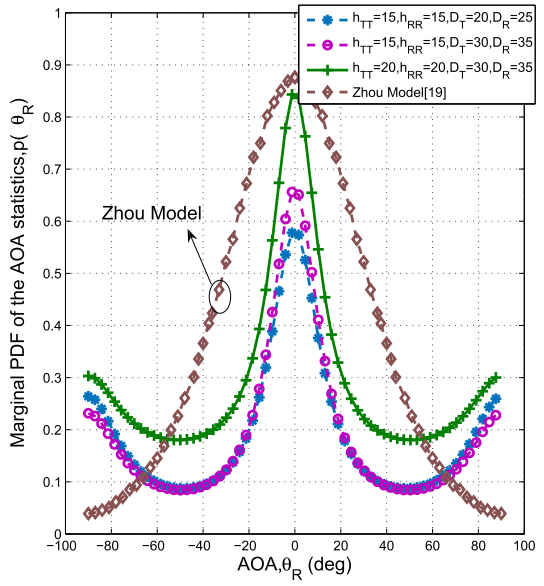

FIGURE 12. PDFs of the AoA statistics in the elevation plane when $h_T = h_R = 5$ m.

increases rapidly, and then decreases slowly after reaching the peak. Moreover, when h_{TT} and h_{RR} are reduced, the scattering range of the emission angle is reduced so that the distribution range of the corresponding PDF of the AoD is also narrowed, as shown in the second set of curves in Fig. 9. Furthermore, when D_T and D_R are increased, the scattering area is elongated so that the corresponding PDF of the AoD around the zero point increases, as shown in the third set of curves in Fig. 9. Ghoraishi [33] conducted a survey on the transmission channels in the city streets of Tokyo and Yokohama, and obtained a series of experimental data. The fourth set of curves shows the power distribution of the transmitter at a measurement scene in the center of Yokohama. The trend is similar to the PDFs of the AoD of our model in Fig. 9, which further verifies the feasibility of the proposed model.

When changing the distances D_T and D_R and the scattering areas based on the geometric channel models in Figs. 2 and 7, the distribution of PDFs of the AoA in the azimuth plane is illustrated in Fig. 10. In the positive axis, the curves increase from zero to the local maximum, and then gradually decrease to the minimum. They then continue to show an upward trend. In the negative axis, the curves gradually fall to a local minimum, and then show an upward trend. Moreover, it can be found that, when changing the distance parameter and the scattering region, the PDF values tend to be equal near zero and the difference becomes larger in the large angle range. The fifth set of curves shows the receiver's power profile detected for a measurement scenario in the center of Yokohama. It can be seen that the PDFs in Fig. 10 have similar distributions, which demonstrates the accuracy of the proposed MIMO model.

The PDFs of the AoD in regard to the distances D_T and D_R and the scattering areas on the elevation level are shown in Fig. 11. Note that the PDF curves are symmetric with respect to the zero point, owing to the symmetry of the geometric model in 3D space. It is obvious that the PDFs tend to decline as the distances D_T and D_R and the scattering areas h_{TT} and h_{RR} decrease, and show a rising trend for $-\pi/2 \leq \theta_T \leq 0$ and a downward trend for $0 \leq \theta_T \leq \pi/2$. Additionally, the PDF distribution fits very well with the Petrus model [7] when an omnidirectional antenna is utilized to the mobile transmitter. Furthermore, the distribution trend is smoother in the small angle range of $[-20°, 20°]$, and the PDF values are more focused near zero, showing the superiority of the proposed model.

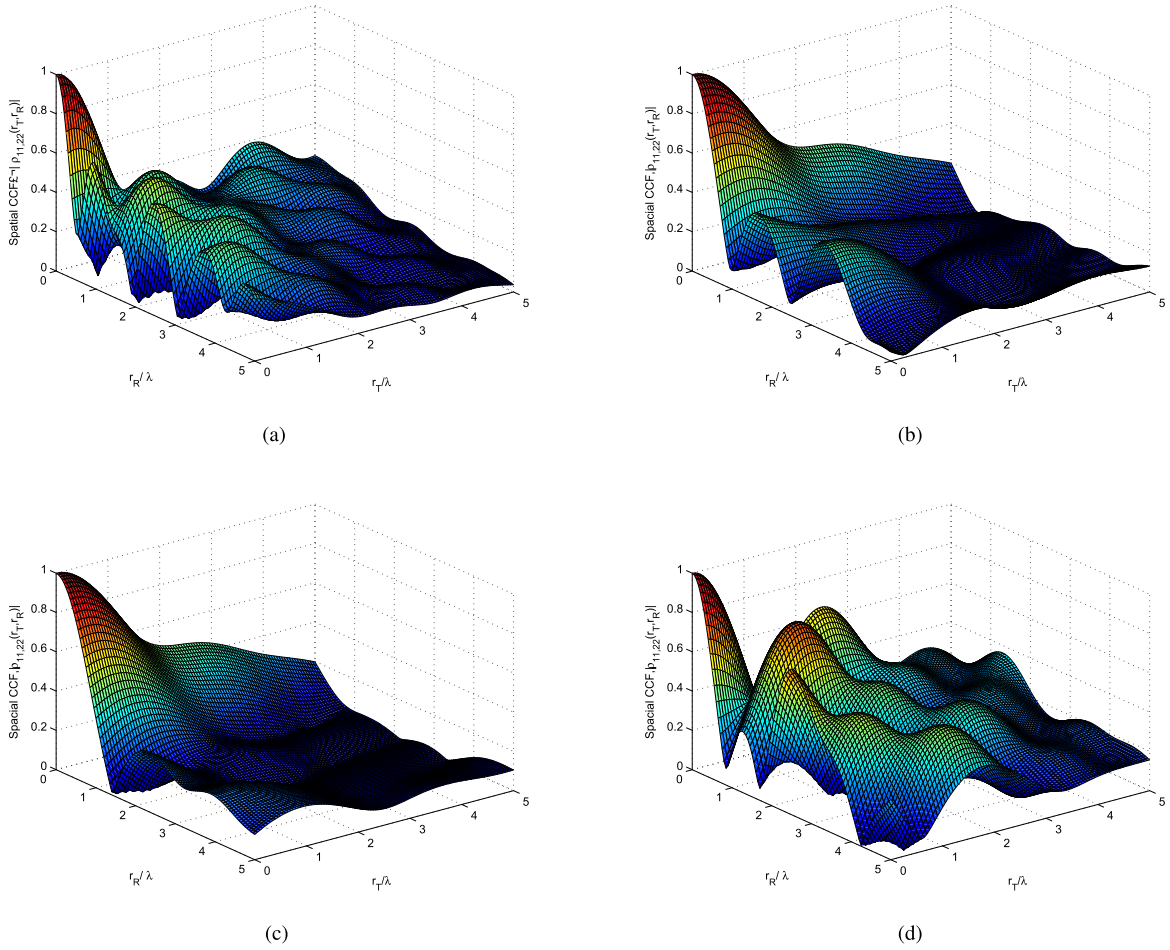

FIGURE 13. Space cross-correlations of the reference channel model when $p = q = 1$, $p' = q' = 2$, and $h_T = h_R = 5$ m.

Fig. 12 presents the PDFs of the AoA in regard to the distances D_T and D_R and the scattering areas on the elevation level. It can be observed from the figure that the PDF curves are also symmetric with respect to the zero point, and that they reach the maximum at zero. Further, there are two troughs at $\theta_R = -\pi/4$ and $\theta_R = \pi/4$, and a rising trend is observed during $-\pi/2 \leq \theta_R \leq -\pi/4$ and $\pi/4 \leq \theta_R \leq \pi/2$. It can also be seen that, unlike the scattering arc region distribution, changes in the distance D_T and D_R do not have a large effect on the AoA statistics, as shown in the first and second sets of curves in Fig. 12. Additionally, the results of the PDF distributions of our model show good agreement with the simulation results in the Zhou model [19] for outdoor V2V street communication scenarios, which confirms the accuracy of theoretical values and the feasibility of describing the outdoor street V2V propagation environments.

C. SPATIAL AND TEMPORAL CROSS-CORRELATIONS

The distributions of the space cross-correlation between the path ($p = q = 1$) and the path ($p' = q' = 2$) for the MIMO antenna array model, with respect to the distances D_T and D_R and the scattering areas h_{TT} and h_{RR}, are shown in Fig. 13. We can see from Fig. 13(a) that the spatial correlation function declines with an oscillating trend, with an increase in the array spacing r_T and r_R, and eventually reaches a relatively stable value, which fits the previous experience well. It is also observed that when the element spacing is half an integer multiple of λ, the spatial cross-correlation takes the peak value; while the element spacing is an integer multiple of λ, the cross-correlation takes the valley value. Moreover, it can be noted that, when the distances D_T and D_R increase and the scattering areas h_{TT} and h_{RR} decrease, the distributions of the spatial CCFs tend to be smoother. The simulation results show good consistency with the Patzold model [21] and provide useful theoretical guidance in the arrangement of element arrays for the optimization of the MIMO multiantenna systems.

Fig.14 presents the distribution of temporal cross-correlations with respect to the variations in antenna elements for the proposed MIMO channel model. It is clearly observed that the temporal cross-correlations decrease rapidly, almost within the short delay of 0.05 s, and then decline in a fading trend, finally reaching a steady value. Besides, for the areas of the upper and lower hemispheres, seen in Fig. 5,

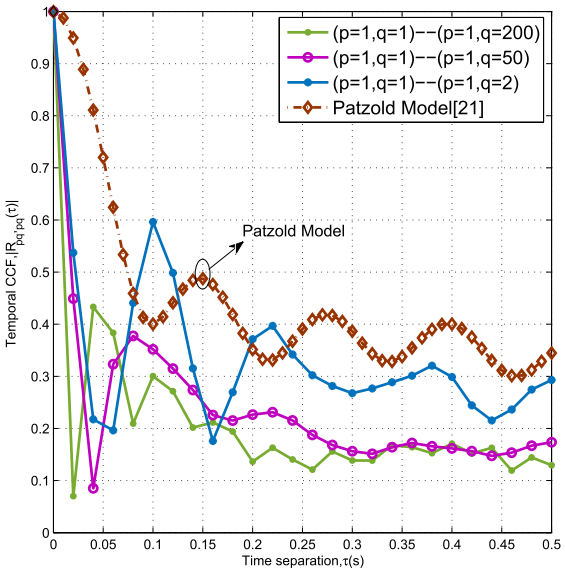

FIGURE 14. Time cross-correlations with respect to different antenna elements when $f_{\max}^{T} = f_{\max}^{R} = 201$ Hz, $h_T = h_R = 5$ m, $h_{TT} = h_{RR} = 20$ m, $D_T = 30$ m, $D_R = 35$ m, and $v_R = 0$.

the correlation gradually decreases when the antenna element q' is changed from 2 to 200, which is also consistent with the actual experience. The results of the proposed model are compared with the data from the Patzold model in [21], which have a unique advantage in this respect, indicating that the model can be utilized in specific outdoor V2V wireless communication scenarios.

V. CONCLUSION

In this paper, we have presented a novel MIMO channel model for congested curved-street V2V NLOS communication environments, assuming that the terminals are equipped with 3D massive MIMO antenna arrays. To evaluate the overall performance of the proposed multiantenna system, we applied the proposed low-elevation massive MIMO antenna arrays to the MT and MR of the built vehicular MIMO channel model, resulting in variations in the AoD and AoA statistics, and the temporal and spatial CCFs. The results exhibited good consistency with the previous channel models and better performances in terms of channel correlations, which validated the generalization of the proposed MIMO channel model and laid a good theoretical foundation for future discussion of 5G MIMO V2V communications. As future work, we plan to consider polarized antenna arrays and antenna-lobe pattern analyses in the extensions of the proposed channel model.

REFERENCES

[1] H. J. Huang, G. Gui, Z. Yang, J. H. Zhang, H. Sari, and F. Adachi, "Deep learning for physical-layer 5G wireless techniques: Opportunities, challenges and solutions," *IEEE Wireless Commun. Mag.*, to be published.
[2] H. Jiang, Z. Zhang, and G. Gui, "Three-dimensional non-stationary wideband geometry-based UAV channel model for A2G communication environments," *IEEE Access*, vol. 7, pp. 26116–26122, 2019.
[3] Q.-U.-A. Nadeem, A. Kammoun, M. Debbah, and M.-S. Alouini, "Design of 5G full dimension massive MIMO systems," *IEEE Trans. Commun.*, vol. 66, no. 2, pp. 726–740, Feb. 2018.
[4] H. Huang, Y. Song, J. Yang, G. Gui, and F. Adachi, "Deep-learning-based millimeter-wave massive MIMO for hybrid precoding," *IEEE Trans. Veh. Technol.*, vol. 68, no. 3, pp. 3027–3032, Mar. 2019.
[5] Y. S. Cho, J. Kim, W. Y. Yang, and C. G. Kang, "The wireless channel: Propagation and fading," in *MIMO-OFDM Wireless Communications With MATLAB*. Hoboken, NJ, USA: Wiley, 2010. [Online]. Available: https://ieeexplore.ieee.org/document/5676095
[6] R. B. Ertel and J. H. Reed, "Angle and time of arrival statistics for circular and elliptical scattering models," *IEEE J. Sel. Areas Commun.*, vol. 17, no. 11, pp. 1829–1840, Nov. 1999.
[7] P. Petrus, J. H. Reed, and T. S. Rappaport, "Geometrical-based statistical macrocell channel model for mobile environments," *IEEE Trans. Commun.*, vol. 50, no. 3, pp. 495–502, Mar. 2002.
[8] H. Jiang, Z. Zhang, and G. Gui, "A novel estimated wideband geometry-based vehicle-to-vehicle channel model using AoD and AoA estimation algorithm," *IEEE Access*, to be published.
[9] X. Cheng, C. X. Wang, D. I. Laurenson, S. Salous, and A. V. Vasilakos, "An adaptive geometry-based stochastic model for non-isotropic MIMO mobile-to-mobile channels," *IEEE Trans. Wireless Commun.*, vol. 8, no. 9, pp. 4824–4835, Sep. 2009.
[10] Y. Wang, M. Liu, J. Yang, and G. Gui, "Data-driven deep learning for automatic modulation recognition in cognitive radios," *IEEE Trans. Veh. Technol.*, to be published.
[11] S. J. Nawaz, B. H. Qureshi, and N. M. Khan, "A generalized 3-D scattering model for a macrocell environment with a directional antenna at the BS," *IEEE Trans. Veh. Technol.*, vol. 59, no. 7, pp. 3193–3204, Sep. 2010.
[12] H. Jiang, J. Zhou, and H. Kikuchi, "Angle and time of arrival statistics for a 3-D pie-cellular-cut scattering channel model," *Wireless Pers. Commun.*, vol. 78, no. 2, pp. 851–865, 2014.
[13] J. Zhou, H. Jiang, and H. Kikuchi, "Generalised three-dimensional scattering channel model and its effects on compact multiple-input and multiple-output antenna receiving systems," *IET Commun.*, vol. 9, no. 18, pp. 2177–2187, 2015.
[14] Y. Yuan, C.-X. Wang, X. Cheng, B. Ai, and D. I. Laurenson, "Novel 3D geometry-based stochastic models for non-isotropic MIMO vehicle-to-vehicle channels," *IEEE Trans. Wireless Commun.*, vol. 13, no. 1, pp. 298–309, Jan. 2014.
[15] S. Kwon and G. L. Stuber, "Cross-polarization discrimination in vehicle-to-vehicle channels: Geometry-based statistical modeling," in *Proc. IEEE Global Telecommun. Conf. (GLOBECOM)*, Dec. 2010, pp. 1–5.
[16] S. C. Kwon, G. L. Stüber, A. V. López, and J. Papapolymerou, "Geometrically based statistical model for polarized body-area-network channels," in *Proc. 10th Int. Symp. Wireless Commun. Syst. (ISWCS)*, Aug. 2013, pp. 1–5.
[17] T. L. Marzetta, "Noncooperative cellular wireless with unlimited numbers of base station antennas," *IEEE Trans. Wireless Commun.*, vol. 9, no. 11, pp. 3590–3600, Nov. 2010.
[18] N. Avazov and M. Patzold, "A geometric street scattering channel model for car-to-car communication systems," in *Proc. Int. Conf. Adv. Technol. Commun. (ATC)*, Aug. 2011, pp. 224–230.
[19] Z. Jie, Y. L. Yao, G.-F. Shao, X.-Y. Shen, and L. Peng, "An electromagnetic street scattering channel model for outdoor vehicular-to-vehicular communication systems," *Acta Phys. Sinica*, vol. 65, no. 14, pp. 1–11, 2016.
[20] W. Chen, Z. Y. He, and T. R. Yao, "A street reference model of MIMO vehicle-to-vehicle fading channel," in *Proc. 3rd IEEE Conf. Ind. Electron. Appl.*, Jun. 2008, pp. 275–278.
[21] N. Avazov and M. Pätzold, "A novel wideband MIMO car-to-car channel model based on a geometrical semi-circular tunnel scattering model," *IEEE Trans. Veh. Technol.*, vol. 65, no. 3, pp. 1070–1082, Mar. 2016.
[22] H. Jiang, Z. Zhang, J. Dang, and L. Wu, "A novel 3-D massive MIMO channel model for vehicle-to-vehicle communication environments," *IEEE Trans. Commun.*, vol. 66, no. 1, pp. 79–90, Jan. 2018.
[23] C. Hong, G. E. Kim, and B.-W. Kim, "Usability analysis of collision avoidance system in vehicle-to-vehicle communication environment," *J. Appl. Math.*, vol. 2014, no. 3, pp. 1–10, 2014, Art. no. 951214.
[24] C. Hong and B. W. Kim, "Performance improvement of collision warning system on curved road based on intervehicle communication," *Math. Problems Eng.*, vol. 2015, Jul. 2015, Art. no. 838929.
[25] L. Wood and W. S. Hodgkiss, "Understanding the Weichselberger model: A detailed investigation," in *Proc. IEEE Mil. Commun. Conf. (MILCOM)*, San Diego, CA, USA, Nov. 2008, pp. 1–7.

[26] S. K. Yong and J. S. Thompson, "Three-dimensional spatial fading correlation models for compact MIMO receivers," *IEEE Trans. Wireless Commun.*, vol. 4, no. 6, pp. 2856–2869, Nov. 2005.
[27] M. Liu, J. Yang, T. Song, J. Hu, and G. Gui, "DSF-NOMA: UAV-assisted emergency communication technology in a heterogeneous Internet of Things," *IEEE Internet Things J.*, to be published.
[28] D. H. Tang, G. F. Shao, J. Zhou, and H. Kikuchi, "A novel MIMO channel model for vehicle-to-vehicle communication system on narrow curved-road environment," *Wireless Pers. Commun.*, vol. 98, no. 4, pp. 3409–3430, 2018.
[29] J. Zhou, H. Jiang, and H. Kikuchi, "Performance of uniform concentric circular arrays in a three-dimensional spatial fading channel model," *Wireless Pers. Commun.*, vol. 83, no. 4, pp. 2949–2963, 2015.
[30] S. Wu, C.-X. Wang, M. Aggoune, M. M. Alwakeel, and Y. He, "A non-stationary 3-D wideband twin-cluster model for 5G massive MIMO channels," *IEEE J. Sel. Areas Commun.*, vol. 32, no. 6, pp. 1207–1218, Jun. 2014.
[31] S. Wu, C. X. Wang, H. Haas, E. H. M. Aggoune, M. M. Alwakeel, and B. Ai, "A non-stationary wideband channel model for massive MIMO communication systems," *IEEE Trans. Wireless Commun.*, vol. 14, no. 3, pp. 1434–1446, Mar. 2015.
[32] A. Ghazal *et al.*, "A non-stationary IMT-advanced MIMO channel model for high-mobility wireless communication systems," *IEEE Trans. Wireless Commun.*, vol. 16, no. 4, pp. 2057–2068, Apr. 2017.
[33] M. Ghoraishi, J.-I. Takada, and T. Imai, "Microcell urban propagation channel analysis using measurement data," in *Proc. IEEE 62nd Veh. Technol. Conf. (VTC-Fall)*, vol. 3, Sep. 2005, pp. 1728–1731.

DENGHONG TANG received the B.S. and M.S. degrees in electrical and information engineering from the Nanjing University of Information Science and Technology, Nanjing, China, in 2013 and 2018, respectively. He is currently pursuing the Ph.D. degree with the Institute of Advanced Navigation and Electromagnetics, Xi'an University of Technology, Xi'an, China. His current research interests include vehicle-to-vehicle communications, massive multiple-input and multiple-output channel modeling, and signal processing.

XIAOLI XI received the B.S. degree in applied physics from the University of Defense Technology, Changsha, China, in 1990, the M.S. degree in biomedical engineering from Fourth Military Medical University, Xi'an, China, in 1998, and the Ph.D. degree in electrical engineering from Xi'an Jiaotong University, Xi'an, in 2004. She is currently a Professor with the Department of Electric Engineering, Xi'an University of Technology, Xi'an. Her recent research interests include wave propagation, antenna design, and communication signal processing.

JIE ZHOU received the B.S. and M.S. degrees in radio engineering from the Nanjing University of Posts and Telecommunications, Nanjing, China, in 1985 and 1990, respectively, and the Ph.D. degree in information engineering from Gunma University, Maebashi, Japan, in 2001. He is currently a Professor with the Department of Electronic and Electrical Engineering, Nanjing University of Information Science and Technology, Nanjing, China, and also with the Department of Electronic Engineering, Niigata University, Japan. His current research interests include mobile communication theory and applications, radio access networks, and wireless sensor networks.